



Remote sensing study of ozone, NO₂, and CO: some contrary effects of SARS-CoV-2 lockdown over India

Prajwal Rawat¹ · Manish Naja¹

Received: 11 April 2021 / Accepted: 5 November 2021 / Published online: 18 November 2021
© The Author(s), under exclusive licence to Springer-Verlag GmbH Germany, part of Springer Nature 2021

Abstract

Escalating emissions of several air pollutants over South Asia could play a detrimental role in the regional and global atmosphere. Therefore, it is necessary to investigate these emissions within the boundary layer and at higher heights utilizing satellite data that are more inclusionary, where limited in situ observations are available. Here, we utilize the Infrared Atmospheric Sounding Interferometer (IASI), Ozone Monitoring Instruments (OMI), TROPospheric Monitoring Instrument (TROPOMI), and Global Ozone Monitoring Experiment (GOME-2) hyperspectral satellite data to assess the changes in emission sources during Indian lockdown with a primary focus on the tropospheric profiles of ozone and carbon monoxide (CO). A significant reduction (> 20%) in the tropospheric ozone was seen over northern and northeast regions compared to 2018, while a dramatic increase (> 20%) compared to 2019 was seen. The subtropical dynamics mainly contributed to the increased ozone over the northern region. An analysis of the ozone production regime showed mostly NO₂ limited regime over the major part of India and VOC limited regime over thermal power plants regions. Unlike in the boundary layer, where CO showed reduction (15–20%), CO profiles showed a consistent increase (as high as 31%) in the free troposphere over the majority of cities and thermal power plants. The CO total column also showed an increase (~ 20%) over central and western India and a slight decrease (5%) over northern India. Similar to CO, an increase (~ 15%) of NO₂ column over the western region was observed particularly compared to 2019. However, unlike ozone and CO, reduction of tropospheric NO₂ columns was seen over the major part of India, with the highest reduction over northern regions (20–52%). Furthermore, homogeneous yearly differences (> 30%) between OMI and TROPOMI NO₂ observations were also seen distinctly over the remote areas. Contrary to surface-based studies, the present study shows an increase in CO, ozone (decrease), and NO₂ at several locations and in the free troposphere during the lockdown.

Keywords Air pollution · Thermal power plants · Ozone · CO · NO₂ · India · Himalaya

Responsible Editor: Gerhard Lammel

Highlights

- Unlike surface, CO vertical profile shows an increase over most of the Indian region during lockdown.
- NO₂ also shows an increase over the downwind region of central-western coal-based power plants.
- Downward transport significantly altered ozone during lockdown mainly in north India.
- TROPOMI and OMI NO₂ show notable differences (~ 50%) mainly over the remote regions.

✉ Manish Naja
manish@aries.res.in

¹ Aryabhata Research Institute of Observational Sciences, Manora Peak, Nainital 263001, India

Introduction

Exposure to higher concentrations of different trace gases and particulate matter leads to a deteriorating impact on human health (Lelieveld et al. 2013) and crops (Lal et al. 2017). This is of major concern in the developing countries where anthropogenic emissions are shown to be increasing (Akimoto 2003; Li et al. 2017a, b) in the want of economic developments. The hazardous air pollutants cause premature mortality, with the highest mortality rate in the Western Pacific region (~ 46%) and Southeast Asia (~ 25%) (Lelieveld et al. 2013). It has been shown that industrial coal-burning, including thermal power plants, is one of the major sources of air pollution in developing countries like India, apart from biomass burning (Venkataraman et al. 2018; Park and Choi 2016). In addition to the higher pollutant levels, abundant

water vapor and the intense solar radiation in the tropical developing countries further contribute to more OH radicals, hence complex photochemistry, involving several trace gases.

India, the rapidly developing country, is increasing its urbanization and industrialization at a faster rate and adding more anthropogenic emissions (Kurokawa et al. 2013, Kurokawa and Ohara 2020; Kumar et al. 2018; Yarragunta et al. 2021). This is of serious concern in the northern region, where emissions from coal-based power plants, automobiles, industries, extensive agriculture practices, etc. are very significant (Singh and Kaskaoutis 2014; Cusworth et al. 2018; Bhardwaj et al. 2016; Srivastava and Naja 2021). However, there is a slightly lower emission and larger wash-out of pollutants in India's southern part (Viswanadham and Santosh 1989; Rosenfeld et al. 2002).

Due to the recent pandemic, lockdowns over different countries have resulted in reductions in emissions of different atmospheric pollutants. The reduction was very significant over China (Xu et al. 2020; Silver et al. 2020) and somewhat moderate over Europe (Ropkins and Tate 2020) and the USA (Shakoor et al. 2020). Similarly, over India, the surface and space-borne observations of different air pollutants showed the highest decrease for PM_{2.5} and PM₁₀ (40–60%) followed by NO₂ (30–70%) and CO (20–40%) (Singh et al. 2020; Mahato et al. 2020; Biswal et al. 2020; Ravindra, et al. 2021). However, to our knowledge, no study examined the effect of lockdown in the vertical profiles of trace gases over India.

This work presents the changes in ozone and CO at different altitudes along with the columnar study of ozone, CO, and NO₂ during 24 March to 20 April (lockdown period) in 2018, 2019, and 2020 over India. The CO and NO₂, the primary air pollutants, are emitted from both anthropogenic and natural activities. Their major emissions sources are combustion processes, including those from industrial/vehicular/biomass/biofuel, and found in higher abundances around highly populated areas (Lamsal et al. 2013). Atmospheric ozone, a useful stratospheric gas for absorbing harmful UV radiation (Madronich 1993; Gao et al. 2012), is a greenhouse gas (Fishman et al. 1979) and a secondary air pollutant in the troposphere (Desqueyroux et al. 2002; Kim et al. 2013). Apart from photochemical production, ozone concentrations are also altered via meteorology and dynamics, including downward transport of ozone-rich air from the stratosphere (Holton et al. 1995; Park et al. 2012). Hence, ozone concentrations and variabilities are complex and largely depend upon local, regional, and seasonal factors. Furthermore, it has been shown that the ozone variations near the surface are more complex than the primary pollutants during the lockdown period over different regions of the world (Shi and Brasseur 2020; Sicard et al. 2020; Ordóñez et al. 2020; Peralta et al. 2020).

Here, we utilized multi-satellite observations, namely OMI on the Aura satellite (Schoeberl et al. 2006), TROPOMI on the Sentinel-5 Precursor satellite (Veefkind et al. 2012), IASI (Klaes et al. 2007), and IASI+GOME-2 on the MetOp satellite, for tracing pollutant levels vertically and horizontally. The synergic IASI+GOME-2 observation of ozone has a very high sensitivity for the lowermost tropospheric ozone (Cuesta et al. 2013, 2018) and offers a unique capability for observing tropospheric ozone profiles during lockdown. The NO₂ columnar observation from OMI and TROPOMI and the subsequent differences of their retrieval over the Indian region are also presented. Additionally, we have employed the data from the year 2018, apart from the year 2019 that has shown new results in terms of changes in concentrations over different parts of India and minimized the conclusions' biases with respect to a particular year.

Study region, dataset, and methodology

Study region

Figure 1 shows the present study domain (5–35° N and 65–95° E) and the marked locations corresponding to selected twelve cities and four coal-based thermal power plants of India. Figure 1 also demonstrates the National Centers for Environmental Prediction (NCEP) reanalysis-based average wind speed and wind direction for 06 UTC (11:30 IST) at 850 hPa over the study region during the period 24 March to 20 April in 2018, 2019, and 2020. NCEP-based wind analysis shows no significant changes in wind patterns among 2018, 2019, and 2020 with mostly regional localized and low-magnitude winds near the surface.

IASI CO observations

IASI is a nadir-viewing Michelson interferometer onboard MetOP satellite (Klaes et al. 2007). MetOP is a polar sun-synchronous satellite with a descending node around 09:30 local time. The IASI nadir-viewing instrument senses IR spectrum (3.7 to 15.4 μm, total 8461 channels) and has a horizontal resolution of 12 km at nadir up to 40 km over a swath width of about 2,200 km (Clerbaux et al. 2009; Turquety, et al. 2009). The nadir spectral radiance in the range of 2143 to 2181.25 cm⁻¹ is utilized to retrieve CO. Here, we have utilized the IASI level2 CO profiles. The retrieval of the CO profile is based on the O3M-SAF ULB/LATMOS Fast Optimal Retrievals on Layers for IASI CO (FORLI-CO algorithm (Hurtmans et al. 2012). The CO profile is provided in 19 fixed layers up to 60 km, corresponding to 18 layers from 0 to 18 km of 1 km width, and a top layer between 18 and 60 km. The IASI CO FORLI retrieval has higher

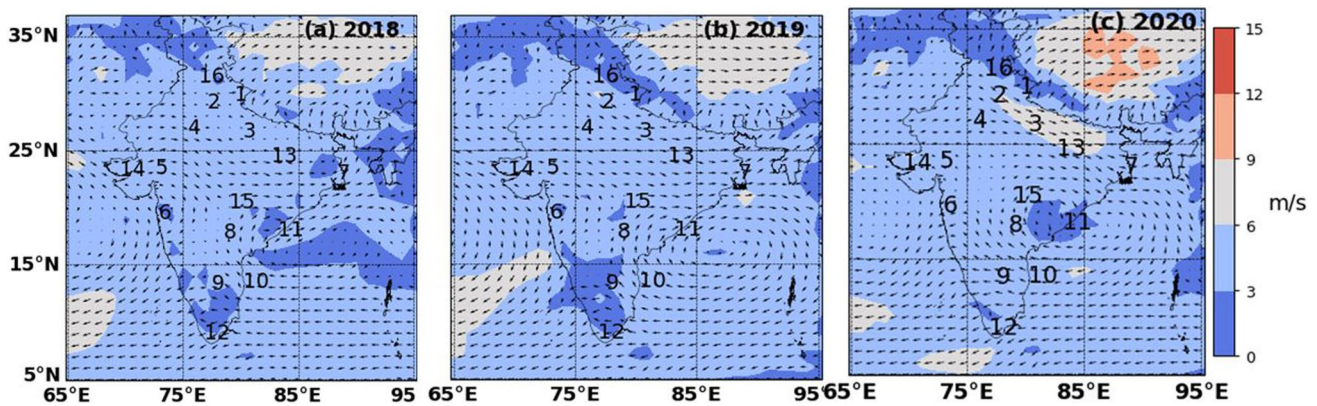


Fig. 1 Average wind speed and direction at 850 hPa during 24 March to 20 April in **a** 2018, **b** 2019, and **c** 2020 based on 06 UTC NCEP-FNL reanalysis data. The numbers indicate cities and thermal power plants (TPPs) namely, (1) Nainital, (2) Delhi, (3) Kanpur, (4) Jaipur,

(5) Ahmedabad, (6) Mumbai, (7) Kolkata, (8) Hyderabad, (9) Bangalore, (10) Chennai, (11) Thiruvananthapuram, (12) Visakhapatnam, (13) Vindhyachal TPP, (14) Mundra TPP, (15) Chandrapur TPP, and (16) Guru Gobind TPP

sensitivity of the retrieved CO around 500 hPa with peaking averaging kernel at this altitude and having retrieval error of less than 10% and 21% in the upper troposphere and lower troposphere, respectively (Wachter et al. 2012). We have used the best quality level 2 CO profiles with a degree of freedom for signal (DOFS) more than 0.5376 (George et al. 2009). Here, the FORLI-CO partial profile (molecules/cm²) of IASI is constructed as follows:

$$\text{CO_CP_CO}_i = \text{CO_CP_CO_A}_i \times \text{CO_X_CO}_i$$

which is further converted to volume mixing ratio (VMR) profile as:

$$\text{CO_VMR_CO}_i = \text{CO_CP_CO}_i \div \text{CO_CP_AIR}_i$$

where i stands for different altitude layers, CO_CP_CO_A is a priori partial columns for CO on each retrieved layer (molecules/cm²), CO_X_CO is scaling vector used for multiplying the a-priori CO vector in order to find the retrieved CO partial profile, and CO_CP_AIR is air partial column on each retrieved layer (molecules/cm²).

OMI NO₂ column observations

The ozone monitoring instrument (OMI), onboard the sun-synchronous polar-orbiting Aura satellite, is a push broom scanning instrument. OMI has an ultraviolet–visible (UV–VIS) spectrometer that measures solar irradiance and the earth’s backscattered radiances at the top of the atmosphere. Its swath width is of 2600 km, enabling global daily coverage with a nadir field-of-view (FOV) of up to 13 km × 24 km. The OMI NO₂ Standard Product (SP) algorithm has utilized the Differential Optical Absorption Spectroscopy (DOAS) (Marchenko et al. 2015; Krotkov et al. 2017; Lamsal et al. 2021). The most recent OMI NO₂

SP, Version 4.0, has been found more reliable and consistent with ground-based and model-based observations (Lamsal et al. 2021), and is minimally affected by modeling artifacts and reduced negative tropospheric NO₂ values (Bucseles et al. 2013). Its validation studies show a general good agreement of its column with lower and higher values to within ± 20% relative to in situ measurements with no consistent seasonal biases (Lamsal et al. 2014, 2021). However, slightly lower columns in urban regions and somewhat higher in the remote areas are observed (Lamsal et al. 2021). We have used the best quality data (VcdQualityFlags = 0) of the OMI tropospheric NO₂ column as in other studies (Goldberg et al. 2017; de Foy et al. 2015).

TROPOMI NO₂, CO, and HCHO column observations

TROPOMI onboard Sentinel-5 Precursor (S-5P) is a more recent and advanced satellite in near-polar sun-synchronous orbit, launched on 13 October 2017 (Veefkind et al. 2012). It is a passive-sensing hyperspectral nadir-viewing imager, flying at an altitude of 817 km, with an ascending node of 13:30 local time and a repeat cycle of 17 days. It has four separate spectrometers, which measure in the ultraviolet (UV), UV–VIS, near-infrared (NIR), and short-wavelength infrared (SWIR) spectral bands. TROPOMI provides both offline and near real-time products for vertical columns of NO₂, HCHO, CO, and other trace gases with a higher spatial resolution around 5.5 to 7.5 km before August 2019 and 3.5 to 5.5 km afterward (Veefkind et al. 2012; Griffin et al. 2019). The retrieval of column densities from TROPOMI L1 UV–VIS radiance and solar irradiance observation is done using the DOAS method (Platt and Stutz 2008). The column L2 offline data of NO₂, CO, and HCHO of better quality (qa_value > 0.7) is used in the present study (Zhao et al. 2020). The TROPOMI retrieved offline product is available after

May 2018; thereby, we could utilize TROPOMI observations in 2019 and 2020 only.

Synergetic IASI + GOME-2 tropospheric ozone observations

Satellite remote sensors utilize spectral response of atmospheric ozone in UV (240–340 nm) and IR (9.6 μm) to observe ozone from space (Worden et al. 2007; Landgraf and Hasekamp 2007). The UV-based satellite measurements are more sensitive for the upper tropospheric and stratospheric ozone; however, the IR-based satellite retrievals relying on the emission/absorption of terrestrial and atmospheric emitted 9.6- μm radiation are more sensitive for the tropospheric ozone. Hence, their synergic observations are used for improved ozone profile retrievals, particularly in the troposphere (Sato et al. 2018; Cuesta et al. 2013).

Here, we have utilized the synergic observation of the IASI and GOME-2 in thermal infrared and ultraviolet, respectively. The co-located morning overpasses of IASI and GOME-2 measurements are used to derive ozone profiles. This unique retrieval technique uses Tikhonov–Phillips-type altitude-dependent constraints, which optimize sensitivity to lower tropospheric ozone. The linearized pseudo-spherical vector discrete ordinate radiative transfer (VLIDORT) and Karlsruhe Optimized and Precise Radiative transfer Algorithm (KOPRA) radiative transfer models are used for simulating UV reflectance and TIR radiance, and the successive retrieval is accompanied by a priori based cost-minimization of solutions (Rodgers 1976, 1990) as discussed in details in Cuesta et al. (2013). The novelty of this synergic IASI + GOME-2 observation is that it is capable of observing the horizontal distribution of ozone pollution plumes located below 3 km (Fig. 2) of altitude in the lower troposphere with a mean bias of 1% and a precision of 16% (Cuesta et al. 2013). IASI + GOME-2 retrieval output shows a higher degree of freedom of signal (DOFS) over the Indian region during 2018, 2019, and 2020, of average values 4.87, 4.85, and 4.88, respectively, with peaking averaging kernels, even in lower troposphere (Fig. 2). The tropospheric ozone column is also derived utilizing IASI and GOME-2 observations by integrating ozone profiles from surface to tropopause, where the thermal tropopause height was taken from IASI observations (Barret et al. 2020).

Results and discussions

Impact on CO over Indian regions: observations from IASI and TROPOMI

The CO total column observations from TROPOMI re-gridded to $1^\circ \times 1^\circ$ resolution were analyzed for the Indian

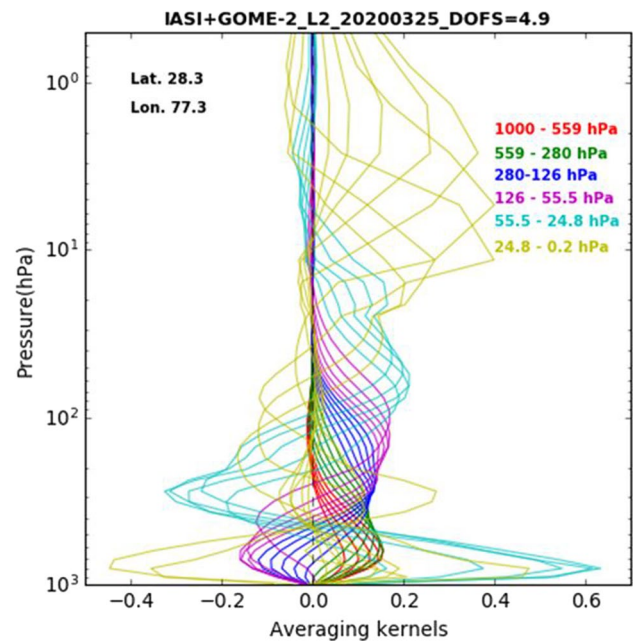


Fig. 2 Typical averaging kernel and corresponding degree of freedom of signal (DOFS) for IASI+GOME-2 vertical ozone profile on 25 March 2020. Higher sensitivity or notable a priori independent ozone retrieval can be seen even at the lower troposphere

lockdown period (24 March to 20 April) in 2019 and 2020 (Fig. 3). Higher concentrations of CO ($> 3.0 \times 10^{18}$ molecule/ cm^2) were observed over central-eastern India, apart from western coastal regions. During the lockdown, a reduction of CO total column is seen over the Indo-Gangetic plain (IGP) and some parts of southern India and the southern Arabian Sea by more than 5%. In contrast, an increase (more than 20%) in CO total column is observed over the central and western regions, including the northern Arabian Sea (Fig. 3c). The increase in CO over central and west India seems to be contributed more from the coal-based thermal power plants (TPPs) around these regions; however, higher lifetime and influence from transport cannot be neglected. Surface-based observation also reported a relatively higher CO mixing ratio (141%) over a western site Dewas during the Indian lockdown (Navinya et al. 2020). Later, it will be discussed that there has been an increase in power generation and production capacities in the central-western thermal power plants during the year 2020.

Figure 4 shows IASI CO vertical profiles over twelve cities and the four largest thermal power plants of India during 24 March to 20 April in 2018, 2019, and 2020. CO mixing ratios are generally found to be lesser (as low as 20%) in the boundary layer during 2020, while they are greater (more than 20%) above the boundary layer when compared with 2019 and 2018. This feature is more prominent in Western India (Ahmedabad, Mumbai, and Mundra TPP) apart from Hyderabad. Increase (5–15%) in CO is also observed over

Fig. 3 TROPOMI total CO observed in **a** 2019 and **b** 2020 during lockdown period (24 March to 20 April) in India. **c** The percentage difference between 2020 and 2019 is also shown

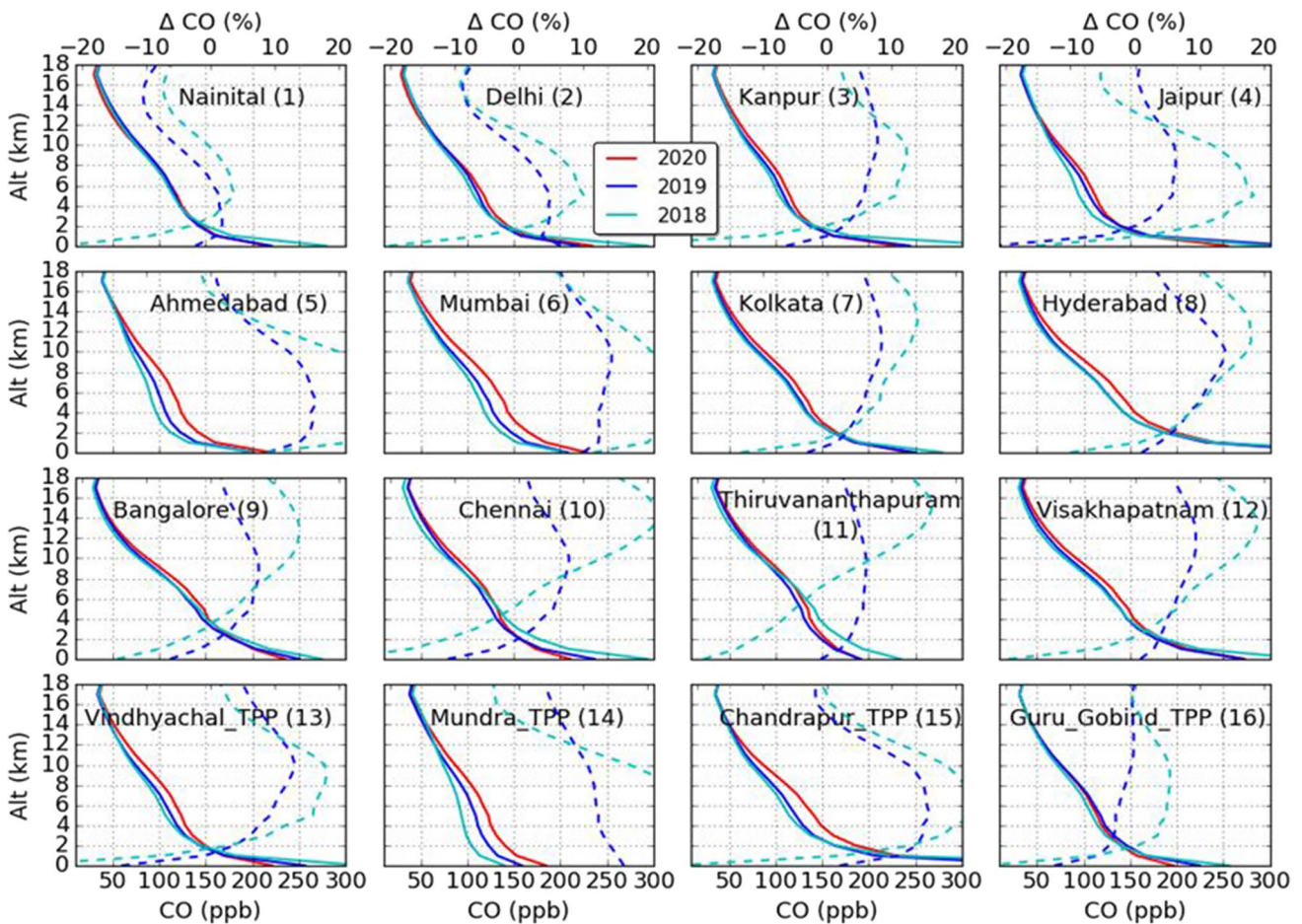
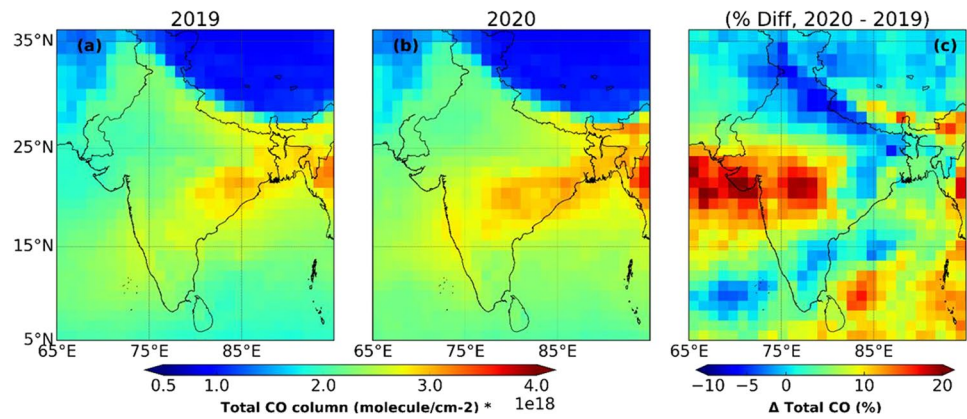


Fig. 4 IASI CO profiles over twelve Indian cities and four major thermal power plants during March 24 to April 20 that correspond to the lockdown period of 2020. Corresponding percentage differences with

respect to 2019 in dotted blue and with 2018 dotted cyan lines are also shown. The number in the bracket shows the cities/TPPs location over India based on Fig. 1

the northern regions, up to the middle troposphere, which reduces in the upper troposphere (Fig. 4 top panel). Near the surface, the maximum mixing ratio of CO (> 300ppbv) was observed over Hyderabad, Visakhapatnam, and most of the TPP. Similar to the profile observations, the CO total column obtained from TROPOMI (Fig. 3) shows an increase over

western and central India and a decrease over northern India as compared to 2019.

The increased CO mixing ratio at various altitudes and the increased CO total column over western and central India are suggested to be due to the increased production capacity of western-central TPPs. For example, the Chandrapur TPP

(biggest TPP in Mumbai with a capacity of 3340 MW) had increased its Plant Load Factor (PLF, a measure of plant capacity utilization) by more than 3% during March 2020 compared to 2019 (<https://npp.gov.in/dailyCoalReports>); besides, fire counts were also higher (Fig. S3) over western regions (Fig. S3). It is observed that the fire counts over India (Fig. S3) have been greater during 2018 (2406), followed by the year 2019 (2172) and 2020 (2047). Furthermore, surface winds (Fig. 1) and HYSPLIT air trajectory (Fig. S1) show low-magnitude winds and dominant local circulation with little signatures of Indo-Gangetic Plain outflows that could further confine these emissions to the source regions of TPPs. Nevertheless, a persistent yearly increase of vertical CO profiles needs more detailed analysis.

Figure 5 shows relative changes in CO in four height layers, namely boundary layer (0–2 km), lower troposphere (2–5 km), middle troposphere (5–10 km), and upper troposphere (10–16 km). In general, CO shows a reduction in the range of 2–21% in the boundary layer (lower panel), except in western regions. However, CO shows a consistent increase (as high as 31%) in the lower troposphere, middle

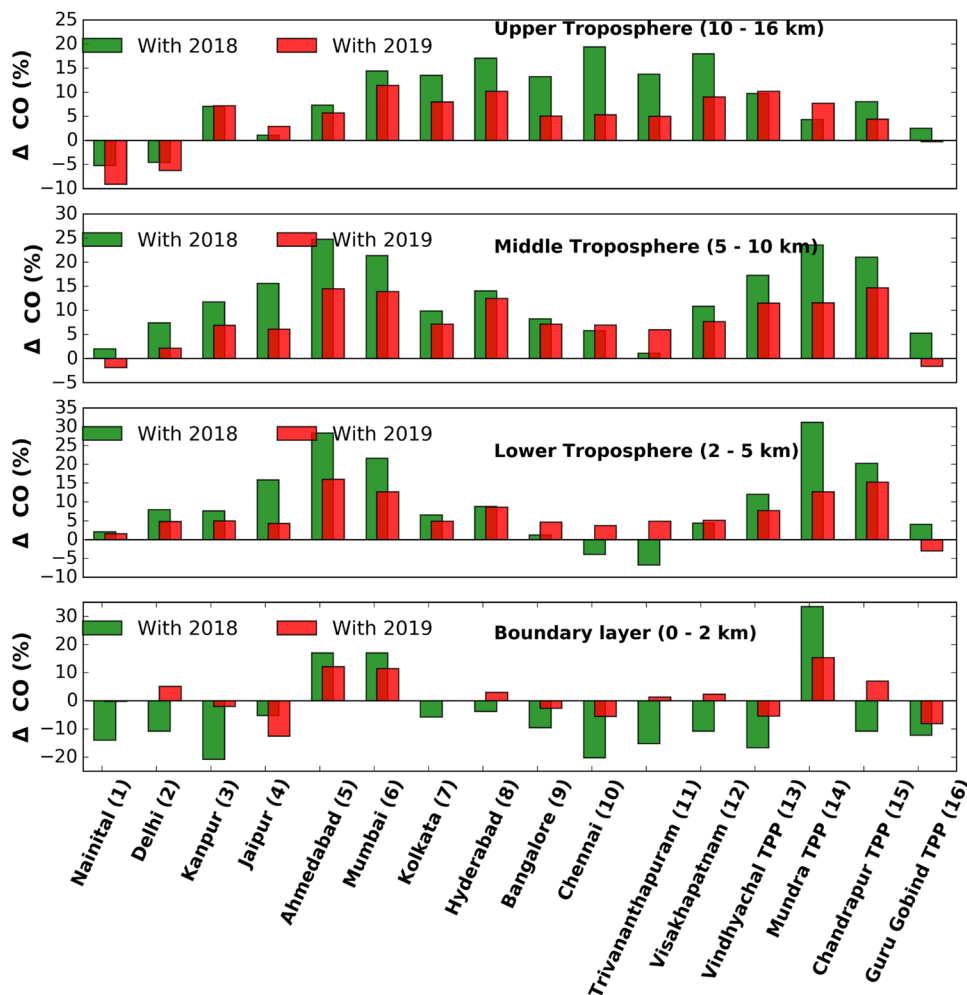
troposphere, and upper troposphere over the majority of Indian regions, including over the thermal power plants regions.

Impact on the tropospheric NO₂ column over Indian regions

The average spatial distributions of the OMI tropospheric NO₂ column during 24 March to 20 April in the years 2018, 2019, and 2020 are shown in Fig. 6. Tropospheric NO₂ columns were seen to be significantly lower (more than 20%) in 2020 when compared with the same period in 2018 and 2019 over Indo-Gangetic plain, northern, central, and eastern India. However, significant increase (> 20%) over western India during 2020 was seen distinctly with respect to 2019.

In addition to OMI, the spatial distribution of tropospheric NO₂ columns was also studied using TROPOMI data (Fig. 7), the more recent and advanced instrument onboard Sentinel-5p with higher ground resolution. TROPOMI shows higher NO₂ concentration over the central, eastern, and some parts of northern India during 2019, similar to

Fig. 5 IASI CO percentage difference [(2020—ref_year)/ref_year]*100 at different altitudes with respect to 2019 and 2018. We have divided the atmosphere in boundary layer (0–2 km), lower troposphere (2–5 km), middle troposphere (5–10 km), and upper troposphere (10–16 km)



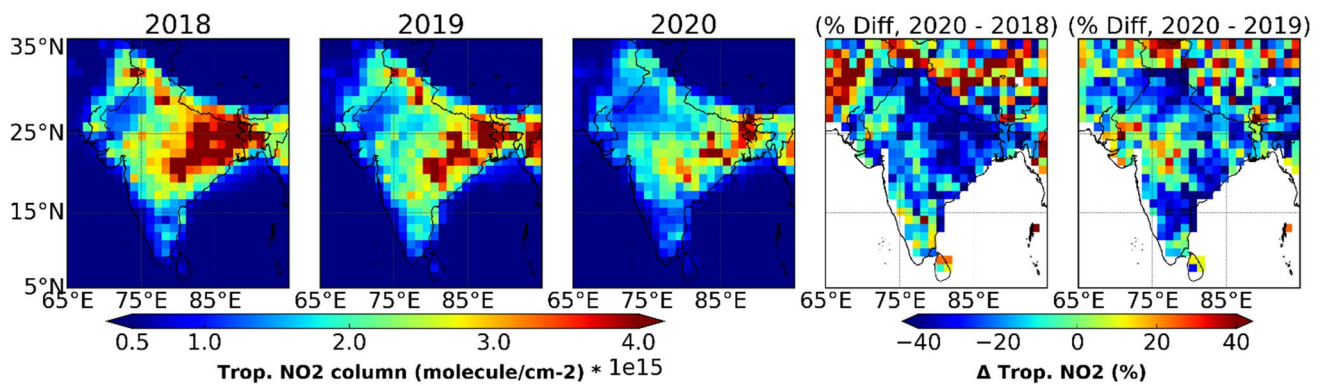


Fig. 6 Tropospheric OMI NO₂ spatial distribution (re-gridded to coarser 1°×1° resolution) observed over India during 24 March to 20 April in 2018, 2019, and 2020. Percentage changes in NO₂ during 2020, with respect to 2018 and 2019, are also shown

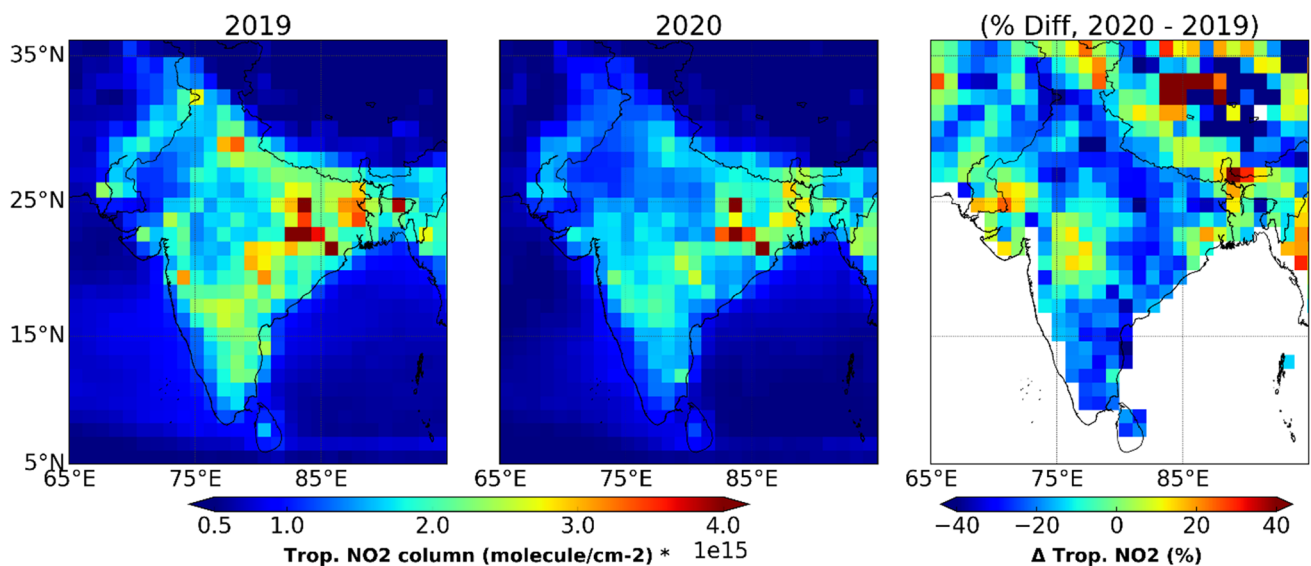


Fig. 7 Tropospheric NO₂ spatial distribution observed from TROPOMI (re-gridded to coarser 1°×1° resolution) over India for 2019 and 2020 lockdown time and their percentage difference

OMI with very sharp source distributions, and exhibits the role of higher spatial resolution over OMI. TROPOMI also shows signatures of increase over the western region (~15%) (Fig. 7), which is also the downwind region of some of the major TPPs with slow winds and dominant local circulation (Fig. S1). Furthermore, the tropospheric NO₂ column is also studied over the selected cities and TPPs (Fig. S2). The largest reduction was seen over the northern and southern cities (20–52%), with the highest reduction over metropolitan city Delhi, about 52% with respect to 2018, as observed by OMI. This reduction is lower when compared with respect to 2019 as observed by OMI (48%) and TROPOMI (31%).

During the lockdown, higher reduction of NO₂ (>20%) in comparison to 2018 was observed over most of the Indian region (Fig. 6). However, in comparison to 2019, the reduction was mostly over northern, eastern, and southern India.

As discussed in the “Impact on CO over Indian regions: observations from IASI and TROPOMI” section, the fire counts have been higher in 2018 followed by in 2019 and 2020. Therefore, biomass burning could have contributed to higher NO₂ in 2018, leading to display of greater reduction in NO₂ during 2020.

Furthermore, higher tropospheric NO₂ columns were observed over central and eastern India during 2018, which subsequently reduced in 2019 and 2020. The central-eastern region is home to various coal-based TPPs (i.e., Rihand TPP, Sipat TPP, Mouda TPP, Farakka TPP, Kahalgaoon TPP), including India’s largest coal-based TPP (Vindhyachal super TPP, installed capacity 4760 MW). An annual report of National Thermal Power Corporation (NTPC) (<https://www.ntpc.co.in/annual-reports/8842/download-complete-annual-report-2018-19>, page no. 21 and <https://www.ntpc.co.in/>

sites/default/files/downloads/44-final-NTPC-AR-30082020.pdf, page no. 35) shows higher gross power generation (megawatt) by more than 5% for 2018 as compared to 2019 for most of these central-eastern TPPs, which could be a possible reason for higher NO_2 in central and eastern India during 2018.

Difference between OMI and TROPOMI over the Indian regions

Figure 8 shows the percentage difference between TROPOMI and OMI tropospheric NO_2 columns over the Indian region. In general higher differences in NO_2 retrieval are observed over the remote location, e.g., the Himalayas, the Arabian Sea, the Bay of Bengal, and coastal areas, apart from central India. The spatial distribution of NO_2 anomalies between both OMI and TROPOMI is more or less consistent in 2019 and 2020. The TROPOMI columnar NO_2 is lower by more than 30% over the Himalayas, the Tibetan plateau, and central India. However, the TROPOMI NO_2 column is higher by more than 40% over the Arabian Sea, the Bay of Bengal, and the coastal region apart from the Himalayan–Tibetan transition belt. A significant difference of more than 50% is also observed between OMI and TROPOMI over remote locations like Nainital in the central Himalaya and coastal cities during 2019 and 2020 (Fig. S2). Such differences between the TROPOMI and OMI over different parts of the world are also discussed in other studies (Bauwens et al. 2020; Wang et al. 2020); however, over India are discussed here.

The possible reason for the difference between the two sensors could be the complex topography over the Himalaya, higher reflectivity of the Tibetan plateau, and cloudy condition over the oceanic regions, which induces notable differences in the retrieval outputs along with retrieval a priories and input parameters (Zhou et al. 2009; Lin et al. 2015). Additionally, space-based sensors are indirect and their retrieval relies on certain algorithms that reflect the higher contribution from retrieval a priories and possess larger errors over the remote locations having lower concentrations. Although OMI and TROPOMI have similar measurement times, the difference among the two sensors might be arising from different a priories (a priories NO_2 profile based on TM5-MP in TROPOMI and GOES-Chem in OMI), other auxiliary information (e.g., surface reflectivity and cloud parameters) as well as differences in cloud masking and other sources of uncertainties in air mass factor calculations. Algorithms for OMI and TROPOMI also differ in the separation of the stratospheric and tropospheric components, which is a significant source of uncertainty in clean background areas. Furthermore, the frequency distribution of TROPOMI and OMI NO_2 shows populated columns around 0.5×10^{15} (molecule/cm²), and the values of populated columns are slightly higher for TROPOMI (Fig. 8, right panel). Furthermore, it can be seen that the number of populated columns (frequency) of about 0.5×10^{15} (molecule/cm²) is higher during the lockdown period as expected in both TROPOMI and OMI observations.

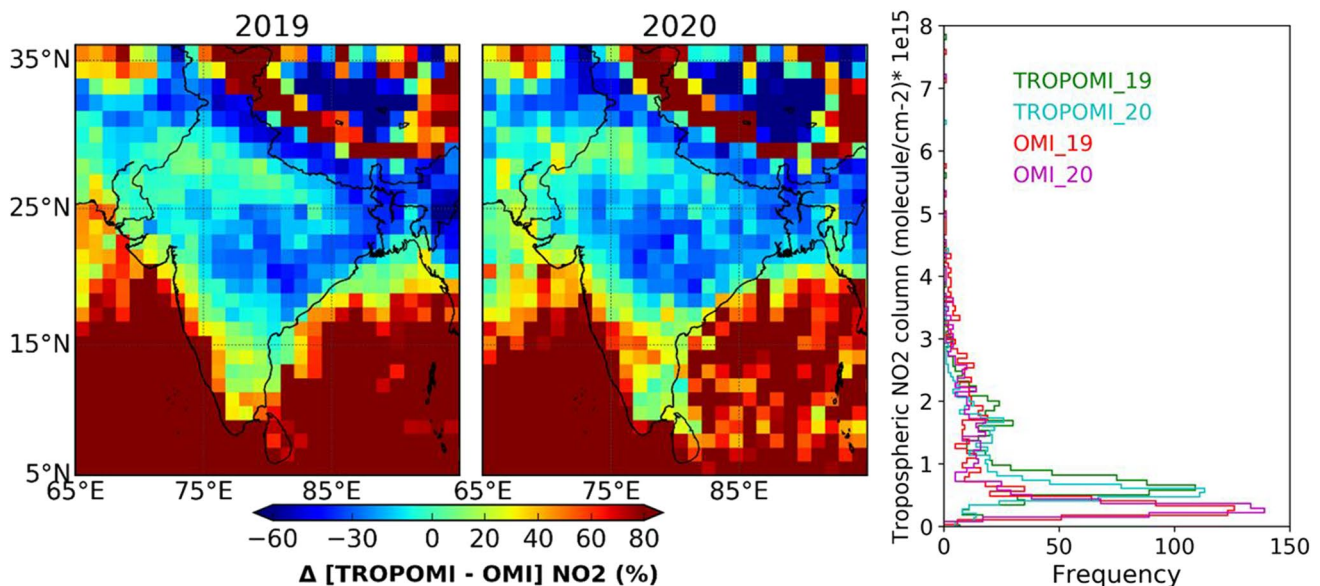


Fig. 8 Percentage difference of tropospheric NO_2 column between OMI and TROPOMI (re-gridded to coarser $1^\circ \times 1^\circ$ resolution) observations $[\frac{\text{TROPOMI} - \text{OMI}}{\text{OMI}} \times 100]$ during 24 March to 20

April in the year 2019 and 2020. Their frequency distribution is also shown in the right panel

Temporal variations in the tropospheric NO₂ and total CO column

The temporal variations in the percentage changes in the tropospheric NO₂ column and total CO column over twelve cities and four thermal power plants are shown in Fig. 9. The tropospheric NO₂ column decreased after lockdown over most of the cities and as high as 45% over Delhi. Similar reductions in NO₂ were also reported worldwide, e.g., a reduction over China up to 54% (Xu et al. 2020), over Europe in the range 30–50% (Ropkins and Tate 2020), over the USA up to 36% (Shakoor et al. 2020), and in India in the range 30–70% (Singh et al. 2020; Biswal et al. 2020). Nevertheless, few Indian cities and TPP regions show some tendency of increase during the lockdown (Fig. 9). Furthermore, over some seaport cities like Chennai, Thiruvananthapuram, and Mumbai, where the significant anthropogenic contribution of NO₂ is also coming from the international and domestic shipping, it shows lower NO₂ concentration before the Indian lockdown and probably reflects the effect of restriction in international shipping before the lockdown began in India.

The total CO column decreased (~5%) over northern regions immediately after lockdown and increased over Ahmedabad, Mumbai, Hyderabad, Mundra TPP, and Chandrapur TPP by more than 10%. However, no significant change was also seen over Kanpur, Jaipur, Kolkata, Visakhapatnam, and Vindhyachal TPP. Southern cities

Bangalore, Chennai, and Thiruvananthapuram showed sharp reduction immediately after lockdown, but both CO and NO₂ columns increased afterward. Such a feature is also seen at Nainital, a high-altitude place in the central Himalayas. Figure 10 shows a time series of tropospheric NO₂ column and total CO column as observed by TROPOMI along with in situ measurement of surface ozone (Sarangi et al. 2014) in 2020. All these gases show a slight reduction just after lockdown but a systematic increase afterward. This increase has been very significant in NO₂ (77%), ozone (67%), and CO (17%) during the lockdown period. Hence, it seems air pollutants in remote regions show a tendency to increase.

Impact on the tropospheric ozone profiles: synergic observation of IASI and GOME-2

The average spatial distribution of ozone during 24 March to 20 April in the years 2018, 2019, and 2020 utilizing synergic observation of IASI and GOME-2 at seven consecutive altitudes (2, 3, 4, 5, 6, 7, and 8 km) is shown in Fig. 11. In general, higher ozone (> 75 ppb) was observed over central India, extending to slightly western and southern regions (Fig. 11r, 11w, 11b1) in the 3 to 5 km altitudes during 2020. This feature is more prominent in 2018, which also extends to the north and northeast regions. The higher ozone concentration over central India decreased systematically with higher altitudes and diminished around 8 km with slightly lower ozone concentration (< 45 ppb), particularly in 2020.

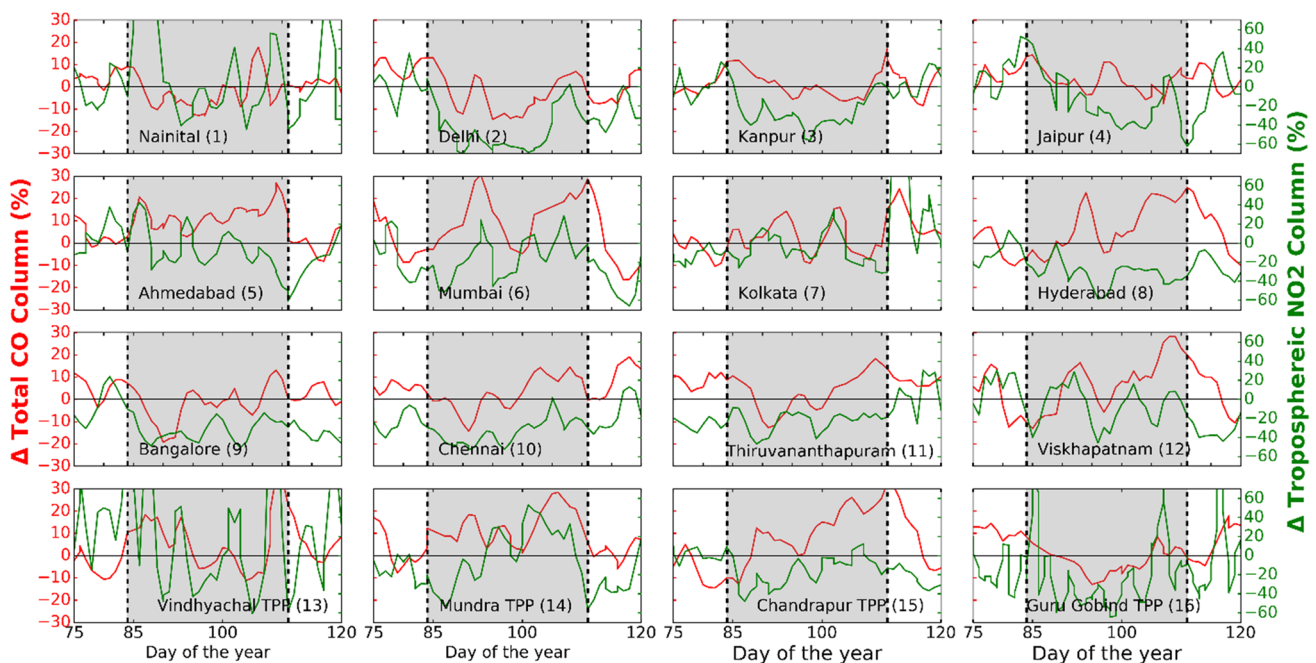
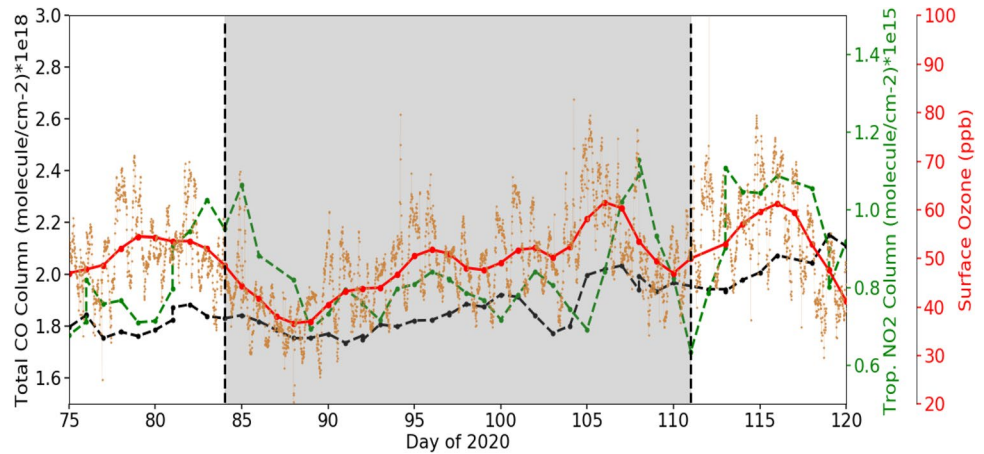


Fig. 9 Temporal variations in percentage changes [(2020–2019)/2019]*100] in total CO column and NO₂ tropospheric column for selected locations. The shaded gray area shows the strict lock-

down period in India (24 March to 20 April 2020). To smoothen the time series, a three day's moving average is used. The number in the bracket shows the cities/TPPs location over India based on Fig. 1

Fig. 10 Time series of tropospheric NO₂ column, total CO column from TROPOMI along with in situ measurement of surface ozone over Nainital in the central Himalayas. Red solid line shows daily average data and the light red dot shows 15-min data of surface ozone



Over the Arabian Sea, high ozone concentrations of more than 75 ppb were observed, particularly at 4 km altitude during 2019 and 2020, which also decreased with higher altitudes. In the 2 km altitude, the ozone concentrations were lower than the adjacent 3 km altitude. The possible region of lower concentrations could be less reliable satellite observations near the surface.

Figure 11 also shows the percentage difference in ozone during 2020 with respect to 2018 and 2019. In comparison to 2018, a decrease of ozone by more than 30% was seen over the northern and northeastern regions, including Indo-Gangetic plain, but an increase (> 15%) is observed over the Arabian Sea and central-western India at all altitudes up to 8 km (second right panel). However, in comparison to 2019, an increase in ozone concentration was observed over central, western, and northern regions by more than 20% and a significant decrease (~20%) over the Indian Ocean (rightmost panel). The increase has been most notable in northern India, and the reduction of ozone over the Indian Ocean is more significant above 5 km altitude. The increased ozone concentration over central and western India in 2020, with respect to 2019, is lower at higher altitudes and it diminishes around 8 km. At the lower altitude region, an increase in ozone is in agreement with an increase in CO (Fig. 4). The increased ozone over the northern region, even at the higher altitudes, exhibits the role of dynamics. The average eternal potential vorticity (EPV) distributions at 600 hPa obtained from MERRA-2 reanalysis data showed a significant increase (> 30%) of EPV for 2020 as compared to 2019 (Fig. S4) over northern India and suggest the contribution of downward transport of ozone in 2020. In addition to satellite observations, balloon-borne observation of ozone over the central Himalayan site shows ozone enhancement episodes even at 3 km altitude during spring 2020, which is discussed in the “[Ozonesonde observations over the central Himalayas](#)” section.

Furthermore, the spatial distribution of average ozone, particularly at 3, 4, 5, and 6 km altitudes in 2018, 2019,

and 2020, is more or less consistent with NO₂ concentrations over India (Fig. 5). The ratio between tropospheric columns of formaldehyde (HCHO) and NO₂ (Fig. 12) over India is studied to assess the ozone production regime. The ratios are mostly above 2.3 in 2019 and 2020. Other studies (Chang et al. 2016; Peralta et al. 2020) have shown that it is a VOC limited regime if HCHO/NO₂ ratio is less than 1.5, while it is NO_x limited regime if HCHO/NO₂ ratio is greater than 2.3. Therefore, there have been strongly NO₂ limited regimes over India during the lockdown period. A signature of VOC limited or transition regimes near the Vindhyachal coal-based thermal power plant and its surroundings is evident. It could also be noted that the ratio is further increased in 2020 as compared to 2019 (Fig. 12). Previous model-based studies (Kumar et al. 2012; Ojha et al. 2012) also showed the NO₂ limited behavior of ozone during spring over the Indian regions.

Additionally, the average ozone profile up to 500 hPa (~6 km) over twelve populated cities and India’s four largest thermal power plants during 24 March to 20 April in 2018, 2019, and 2020 is also studied (Fig. S5). In comparison to 2018, a general decrease in ozone was observed except over Mumbai and Guru Gobind TPP. With respect to 2019, an increase of ozone up to 30% was observed over northern cities and a decrease over the southern cities. Further percentage changes of ozone concentrations in 2020 were studied with respect to 2018 and 2019 for four height layers (Fig. S6). In comparison to 2018, ozone concentration mostly decreased over all selected regions (Table S1) in all layers with relatively higher reduction over the northern cities and slightly lower reduction over the southern cities, except in the upper troposphere. In contrast to 2019, an increase of ozone over the northern, western regions, and thermal power plants (mainly in BL and LT) (Table S1) was seen, apart from a notable decrease (> 5%) in the upper troposphere and a reduction of ozone over the southern region is seen in all layers.

Fig. 11 Spatial distribution of tropospheric ozone at 2, 3, 4, 5, 6, 7, and 8 km altitude from IASI+GOME-2 observations during 24 March to 20 April in years 2018, 2019, and 2020 and their percentage differences are also shown at the two right columns

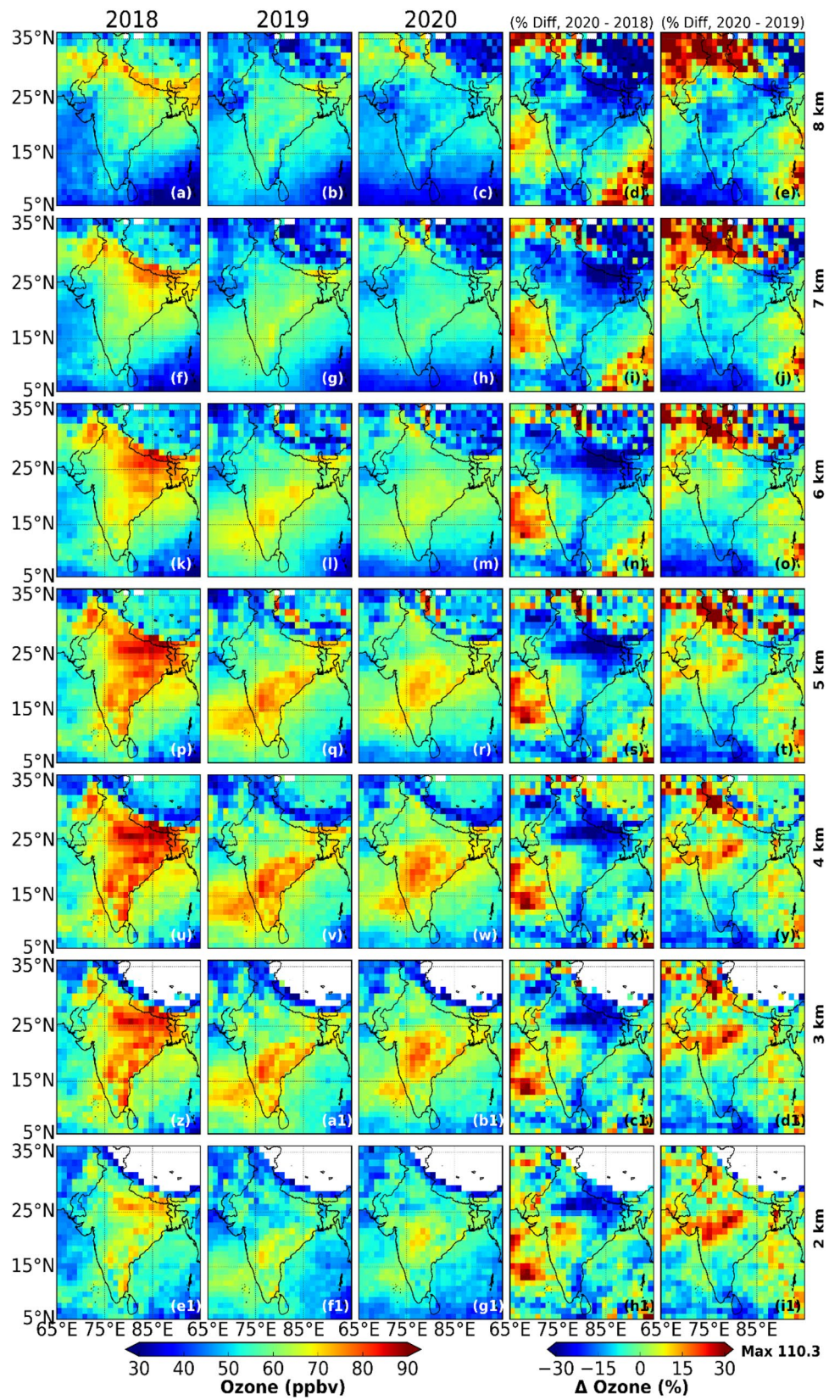


Fig. 12 HCHO/NO₂ ratio from TROPOMI column observations over India. It shows a greater tendency of the NO₂ limited regime during 2020 than in 2019

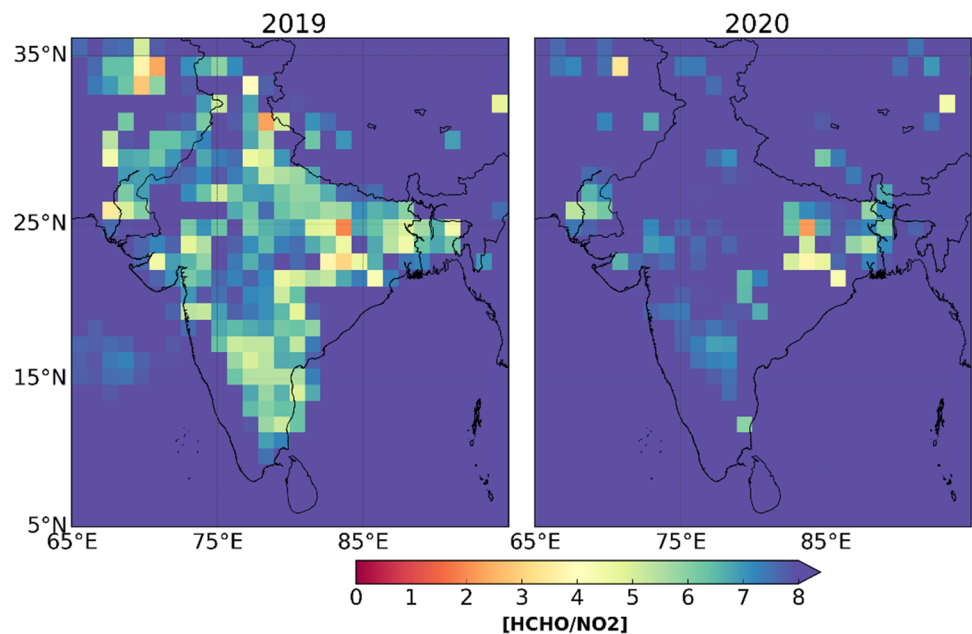


Figure 13 shows the average tropospheric ozone column over India during 24 March to 20 April in 2018, 2019, and 2020. In 2020, a uniformly distributed tropospheric ozone column of about 40 DU was seen over India; however, in 2018 and 2019, a slightly higher column (> 50 DU) over the northern Indo-Gangetic Plain and the northeast region was seen, which is more prominent in 2018. A considerable reduction of tropospheric ozone columns was seen in 2020 over the northern and northeast regions, which is significant (> 15%) compared with 2018. In contrast, an increase of more than 20% is observed over the northern region when compared with 2019. An analysis of the tropospheric ozone column over twelve populated cities and the four biggest TPPs shows the highest column over Vindhyachal TPP (48 DU), Kanpur (46 DU), and Chandrapur TPP (43 DU)

(Fig. S7) in the years 2018, 2019, and 2020, respectively. Mostly decrease of the tropospheric ozone column was seen over the Indian regions similar to the NO₂ except for Nainital and Guru Gobind TPP, which are located in northern India, where apart from precursor's photochemistry, downward transport significantly alters the ozone concentrations (Bhardwaj et al. 2018; Rawat et al. 2020).

Ozonesonde observations over the central Himalayas

Figure 14 shows the average vertical ozone distribution (Ojha et al. 2014; Rawat et al. 2020) observed during March, April, and May over the central Himalayas. We could not conduct ozone soundings in April 2020 due to the nationwide lockdown. April 2020 could have shown

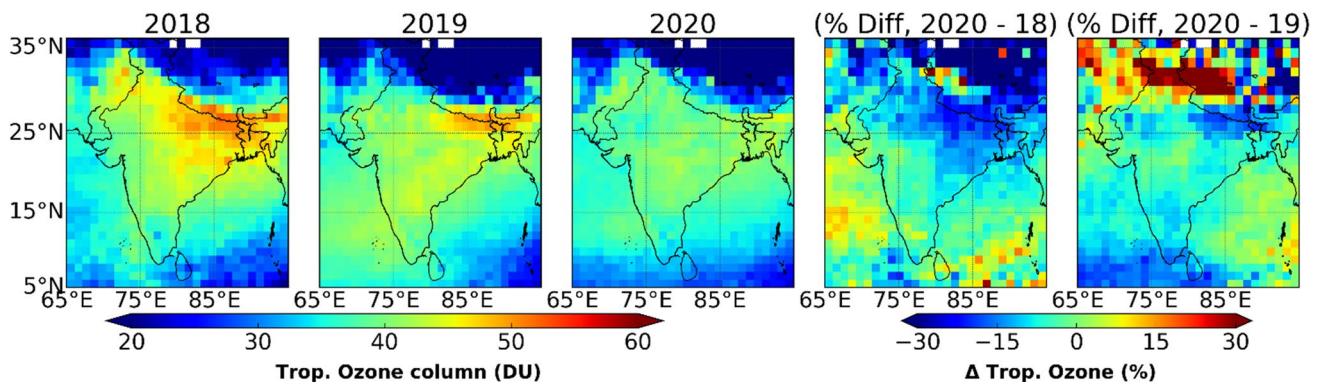


Fig. 13 Tropospheric ozone column over India during 24 March to 20 April in 2018, 2019, and 2020 from IASI+GOME-2 synergic observations. Changes in the tropospheric ozone column are also shown

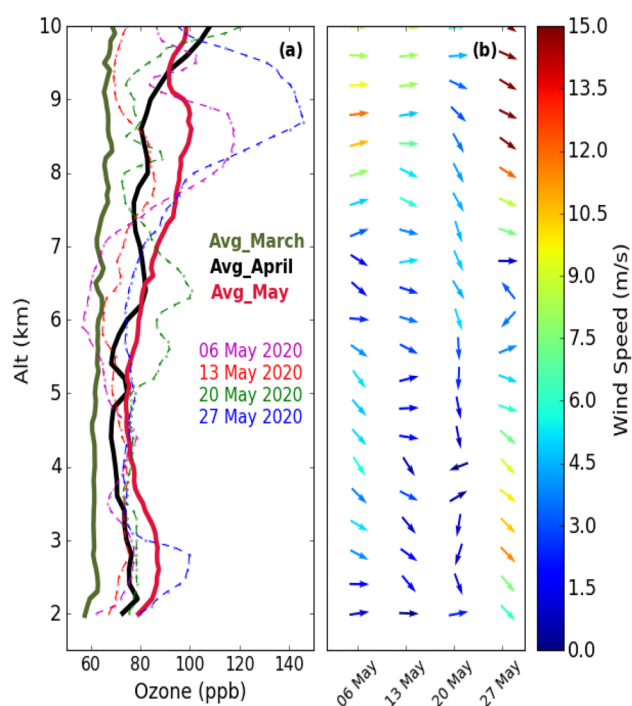


Fig. 14 Average vertical ozone distribution over the central Himalayas during March, April, and May (2011–2019). **a** Four-day ozone profiles during May 2020 and **b** wind observations are also shown. Here, wind speeds are shown by the color bar of the quiver and quiver arrows show wind direction

the best effects of lockdown on ozone profiles, still the less restricted lockdown ozone profiles in May 2020 are studied by making four ozonesoundings (6, 13, 20, 27 May 2020). A successive increase in average ozone could be seen from March to May month in the average profiles (Fig. 14a). In general, during all 4 days in May, ozone distributions are found to be more or less within one sigma variation of May month's average. However, ozone increase is seen on 27 May at around 3 km and 9 km and on 20 May at 5–7 km. Tropospheric NO_2 showed a slight but insignificant decrease on 27 May. The influence of westerly wind seems to play an important role, particularly for 27 May 2020. Strong westerly winds (> 8 m/s and > 15 m/s) were observed near the high ozone altitudes (3 and 9 km) on 27 May 2020 (Fig. 14b). The HYSPLIT trajectory (Fig. S8) analysis also confirms the long-range transport of upper tropospheric air for this high ozone event. In all four ozone profiles of May 2020, higher ozone above 8 km was observed, which could be due to the contribution from the active downward transport over northern regions during spring (Ojha et al. 2014; Naja et al. 2016). Hence, dynamics is likely playing an important role in ozone enhancements, even at lower altitude (~ 3 km) regions.

Summary and conclusions

In 2020, a short-term improvement in the air quality near the surface had been reported from different countries due to the nationwide lockdown. Here, we have analyzed data from space-borne sensors (IASI, OMI, TROPOMI, and GOME-2) to study changes in vertical distribution and columnar values of ozone, CO, and NO_2 during the nationwide lockdown in India that show some contrary results. Furthermore, we have used data of the year 2018, in addition to 2019, which has shown new results while minimizing the conclusions' biases with respect to a particular year. Twelve populated cities and India's largest coal-based thermal power plants were further selected to quantify the effects.

Overall significant reduction of NO_2 (up to 52%) is observed over India, with some enhancement over the downwind regions of coal-based thermal power plants. Unlike NO_2 , ozone and CO concentrations show vastly varying influences of lockdown over India's different areas and in the vertical distributions. In 2020, vertical ozone distribution showed an explicit increase ($> 20\%$) over western and central India, including the Arabian Sea, and a decrease ($\sim 20\%$) over the southern coastal areas compared to both 2018 and 2019. Furthermore, a reduction ($> 30\%$) compared to 2018 and an increase (as high as 110%) compared to 2019 are observed over northern India. Similar to the profile, tropospheric ozone columns also show a considerable reduction ($> 15\%$) over the northern and northeast regions when compared with 2018 and an increase of more than 20% with respect to 2019.

An increase ($\sim 20\%$) in total CO is observed over central and western India and a decrease ($\sim 5\%$) over northern India during the lockdown period, which was consistent with changes seen in ozone. The vertical distribution in CO shows a systematic increase (as high as 31%) in the lower troposphere, middle troposphere, and upper troposphere over the majority of Indian regions, including over the thermal power plants regions. This feature was more prominent over the western regions.

The tropospheric NO_2 columns significantly reduced over most of the Indian regions except the western part, where a notable increase was seen ($\sim 20\%$) during the lockdown. An increase in CO and NO_2 during the lockdown period is suggested to be largely due to increased power production in coal-based thermal power plants (TPPs) that has also induced an increase in ozone. Furthermore, an analysis on the identification of ozone production regime showed an increased tendency of NO_2 limited regime over major parts of India, while VOC limited regime over thermal power plants regions. The columnar changes in NO_2 were more or less agreeable in both OMI and TROPOMI

observations; however, notable differences (> 30%) are also seen over the remote areas, e.g., Tibetan plateau, the central Himalayas, and coastal regions.

Unlike surface-based studies, those have shown a clear decrease in pollutant levels, the present study shows an increase in CO, NO₂, and ozone (decrease) at several locations and at different altitude regions. Lockdown had provided a good opportunity to assess the impact of the coal-based thermal power plants in India, when the majority of other emissions were at nominals. Furthermore, it has been shown that apart from the lockdown impact, the ozone concentration is also altered via dynamical variability, mainly over northern India. This study has used polar-orbiting satellite sensors that have limited temporal coverage over a specific region. It is expected that the recently launched GEMS mission onboard GEO-KOMPSAT-2 satellite will provide proficient observations with the diurnal variations of several trace gases and aerosols over the different Asian countries, including large part of India (Kim et al. 2020) that will lead to better assessments of emissions of many harmful atmospheric pollutants.

Supplementary Information The online version contains supplementary material available at <https://doi.org/10.1007/s11356-021-17441-2>.

Acknowledgements We are grateful to Director ARIES (Prof. Dipankar Banerjee), Prof. Shyam Lal, and Mr. S. Venkataramni for discussions and kindly supporting this work. We acknowledge EUMETSAT and NASA-EARTHDATA online data portals for providing IASI, TROPOMI, and OMI label2 data. The AERIS and IASI joint portal is warmly acknowledged for providing access to the IASI+GOME-2 data and LISA for the development of the retrieval algorithms. Discussion with Dr. Lok N. Lamsal about OMI and TROPOMI NO₂ data is highly acknowledged. We would like to thank Dr. Juan Cuesta and Centre National des Etudes Spatiales for financing the SURVEYPOLLUTION project and the AERIS French data center that support the validation and production of the IASI+GOME2 ozone multispectral satellite product. We would also like to acknowledge the use of the MODIS fire data through FIRMS archive download and the NOAA HYSPLIT model for backward air trajectory data. Help from Deepak and Nitin during balloon launches and coordination by the air traffic control is highly acknowledged. We are thankful to the two reviewers for their constructive comments.

Author contribution PR and MN both have contributed equally in the manuscript preparation.

Funding This work was supported by the ISRO-ATCTM project and ARIES, DST.

Availability of data and materials Satellite data of IASI, TROPOMI, and OMI are available at EUMETSAT and NASA-EARTHDATA online data portals. IASI + GOME-2 data is available at the AERIS and IASI joint portal. MODIS fire data is available at FIRMS website. Back air trajectories are calculated using the NOAA HYSPLIT model. All the processed data, including ozone-sonde, are available, while writing to the corresponding author (manish@aries.res.in).

Declarations

Ethics approval and consent to participate N. A.

Consent for publication N.A.

Competing interests The authors declare no competing interests.

References

- Akimoto H (2003) Global air quality and pollution. *Science* 302(5651):1716–1719
- Barret B, Emili E, Le Flochmoen E (2020) A tropopause-related climatological a priori profile for IASI-SOFRID ozone retrievals: improvements and validation. *Atmos Meas Tech* 13(10):5237–5257
- Bauwens M, Compernelle S, Stavrou T, Müller JF, Van Gent J, Eskes H, Levelt PF, Vander AR, Veeffkind JP, Vlietinck J, Yu H (2020) Impact of coronavirus outbreak on NO₂ pollution assessed using TROPOMI and OMI observations. *Geophys Res Lett* 47(11):e2020GL087978
- Bhardwaj P, Naja M, Kumar R, Chandola HC (2016) Seasonal, interannual, and long-term variabilities in biomass burning activity over South Asia. *Environ Sci Pollut Res* 23(5):4397–4410
- Bhardwaj P, Naja M, Rupakheti M, Lupascu A, Mues A, Panday AK, Kumar R, Mahata KS, Lal S, Chandola HC, Lawrence MG (2018) Variations in surface ozone and carbon monoxide in the Kathmandu Valley and surrounding broader regions during SusKat-ABC field campaign: role of local and regional sources. *Atmospheric Chemistry and Physics* 18(16):11949–11971
- Biswal A, Singh T, Singh V, Ravindra K, Mor S (2020) COVID-19 lockdown and its impact on tropospheric NO₂ concentrations over India using satellite-based data. *Heliyon* 6(9):e04764
- Bucselá EJ, Krotkov NA, Celarier EA, Lamsal LN, Swartz WH, Bhartia PK, Boersma KF, Veeffkind JP, Gleason JF, Pickering KE (2013) A new stratospheric and tropospheric NO₂ retrieval algorithm for nadir-viewing satellite instruments: applications to OMI. *Atmos Meas Tech* 6(10):2607–2626
- Chang CY, Faust E, Hou X, Lee P, Kim HC, Hedquist BC, Liao KJ (2016) Investigating ambient ozone formation regimes in neighboring cities of shale plays in the Northeast United States using photochemical modeling and satellite retrievals. *Atmos Environ* 142:152–170
- Clerbaux C, Boynard A, Clarisse L, George M, Hadji-Lazaro J, Herbin H, Hurtmans D, Pommier M, Razavi A, Turquety S, Wespes C (2009) Monitoring of atmospheric composition using the thermal infrared IASI/MetOp sounder. *Atmos Chem Phys* 9(16):6041–6054
- Cuesta J, Eremenko M, Liu X, Dufour G, Cai Z, Höpfner M, von Clarmann T, Sellitto P, Forêt G, Gaubert B, Beekmann M (2013) Satellite observation of lowermost tropospheric ozone by multispectral synergism of IASI thermal infrared and GOME-2 ultraviolet measurements over Europe. *Atmos Chem Phys* 13(19):9675
- Cuesta J, Kanaya Y, Takigawa M, Dufour G, Eremenko M, Foret G, Miyazaki K, Beekmann M (2018) Transboundary ozone pollution across East Asia: daily evolution and photochemical production analysed by IASI+ GOME2 multispectral satellite observations and models. *Atmos Chem Phys* 18(13):9499–9525
- Cusworth DH, Mickley LJ, Sulprizio MP, Liu T, Marlier ME, DeFries RS, Guttikunda SK, Gupta P (2018) Quantifying the influence of agricultural fires in northwest India on urban air pollution in Delhi, India. *Environ Res Lett* 13(4):044018

- Desqueyroux H, Pujet JC, Prosper M, Squinazi F, Momas I (2002) Short-term effects of low-level air pollution on respiratory health of adults suffering from moderate to severe asthma. *Environ Res* 89(1):29–37
- de Foy B, Lu Z, Streets DG, Lamsal LN, Duncan BN (2015) Estimates of power plant NO_x emissions and lifetimes from OMI NO₂ satellite retrievals. *Atmos Environ* 116:1–11
- Fishman J, Ramanathan V, Crutzen PJ, Liu SC (1979) Tropospheric ozone and climate. *Nature* 282(5741):818–820
- Gao Z, Gao W, Chang NB (2012) Spatial statistical analyses of global trends of ultraviolet B fluxes in the continental United States. *Gisci Remote Sens* 49(5):735–754
- Goldberg DL, Lamsal LN, Loughner CP, Swartz WH, Lu Z, Streets DG (2017) A high-resolution and observationally constrained OMI NO₂ satellite retrieval. *Atmos Chem Phys* 17(18):11403–11421
- George M, Clerbaux C, Hurtmans D, Turquety S, Coheur PF, Pommier M, Hadji-Lazaro J, Edwards DP, Worden H, Luo M, Rinsland C (2009) Carbon monoxide distributions from the IASI/METOP mission: evaluation with other space-borne remote sensors. *Atmos Chem Phys* 9(21):8317–8330
- Griffin D, Zhao X, McLinden CA, Boersma F, Bourassa A, Dammers E, Degenstein D, Eskes H, Fehr L, Fioletov V, Hayden K (2019) High-resolution mapping of nitrogen dioxide with TROPOMI: first results and validation over the Canadian oil sands. *Geophys Res Lett* 46(2):1049–1060
- Holton JR, Haynes PH, McIntyre ME, Douglass AR, Rood RB, Pfister L (1995) Stratosphere-Troposphere Exchange. *Rev Geophys* 33(4):403–439
- Hurtmans D, Coheur PF, Wespes C, Clarisse L, Scharf O, Clerbaux C, Hadji-Lazaro J, George M, Turquety S (2012) FORLI radiative transfer and retrieval code for IASI. *J Quant Spectrosc Radiat Transfer* 113(11):1391–1408
- Kim J, Cho HK, Mok J, Yoo HD, Cho N (2013) Effects of ozone and aerosol on surface UV radiation variability. *J Photochem Photobiol, B* 119:46–51
- Kim J, Jeong U, Ahn MH, Kim JH, Park RJ, Lee H, Song CH, Choi YS, Lee KH, Yoo JM, Jeong MJ (2020) New era of air quality monitoring from space: Geostationary Environment Monitoring Spectrometer (GEMS). *Bull Am Meteor Soc* 101(1):E1–E22
- Klaes KD, Cohen M, Buhler Y, Schlüssel P, Munro R, Luntama JP, von Engeln A, Clérigh EÓ, Bonekamp H, Ackermann J, Schmetz J (2007) An introduction to the EUMETSAT polar system. *Bull Am Meteor Soc* 88(7):1085–1096
- Krotkov NA, Lamsal LN, Celarier EA, Swartz WH, Marchenko SV, Bucselo EJ, Chan KL, Wenig M, Zara M (2017) The version 3 OMI NO₂ standard product. *Atmos Meas Tech* 9:3133–3149
- Kumar R, Naja M, Pfister GG, Barth MC, Wiedinmyer C, Brasseur GP (2012) Simulations over South Asia using the Weather Research and Forecasting model with Chemistry (WRF-Chem): chemistry evaluation and initial results. *Geosci Model Dev* 5:619–648. <https://doi.org/10.5194/gmd-5-619-2012>
- Kumar R, Barth MC, Pfister GG, Delle Monache L, Lamarque JF et al (2018) How will air quality change in South Asia by 2050? *J Geophys Res Atmos* 123(3):1840–1864
- Kurokawa J, Ohara T, Morikawa T, Hanayama S, Janssens-Maenhout G, Fukui T, Kawashima K, Akimoto H (2013) Emissions of air pollutants and greenhouse gases over Asian regions during 2000–2008: regional Emission inventory in ASia (REAS) version 2. *Atmos Chem Phys* 13(21):11019–11058. <https://doi.org/10.5194/acp-13-11019-2013>
- Kurokawa J, Ohara T (2020) Long-term historical trends in air pollutant emissions in Asia: Regional Emission inventory in ASia (REAS) version 3. *Atmos Chem Phys* 20(21):12761–12793
- Lal S, Venkataramani S, Naja M, Kuniyal JC, Mandal TK, Bhuyan PK, Kumari KM, Tripathi SN, Sarkar U, Das T, Swamy YV (2017) Loss of crop yields in India due to surface ozone: An estimation based on a network of observations. *Environ Sci Pollut Res* 24(26):20972–20981
- Lamsal LN, Krotkov NA, Celarier EA, Swartz WH, Pickering KE, Bucselo EJ, Gleason JF, Martin RV, Philip S, Irie H, Cede A (2014) Evaluation of OMI operational standard NO₂ column retrievals using in situ and surface-based NO₂ observations. *Atmos Chem Phys* 14(21):11587
- Lamsal LN, Krotkov NA, Marchenko S, Qin W, Yang E-S, Fasnacht Z, Joiner J, Choi S, Haffner D, Swartz WH, Fisher B, Bucselo E (2021) Ozone Monitoring Instrument (OMI) Aura nitrogen dioxide standard product version 4.0 with improved surface and cloud treatments. *Atmos Meas Tech* 14:455–479. <https://doi.org/10.5194/amt-14-455-2021>
- Lamsal LN, Martin RV, Parrish DD, Krotkov NA (2013) Scaling relationship for NO₂ pollution and urban population size: a satellite perspective. *Environmental science & technology* 47(14):7855–7861
- Landgraf J, Hasekamp OP (2007) Retrieval of tropospheric ozone: The synergistic use of thermal infrared emission and ultraviolet reflectivity measurements from space. *J Geophys Res* 112:D08310. <https://doi.org/10.1029/2006JD008097>
- Lelieveld J, Barlas C, Giannadaki D, Pozzer AJACP (2013) Model calculated global, regional and megacity premature mortality due to air pollution. *Atmos Chem Phys* 13(14):7023–7037
- Li C, McLinden C, Fioletov V, Krotkov N, Carn S, Joiner J, Streets D, He H, Ren X, Li Z, Dickerson RR (2017a) India is overtaking China as the world's largest emitter of anthropogenic sulfur dioxide. *Sci Rep* 7(1):1–7
- Li M, Zhang Q, Kurokawa JI, Woo JH, He K, Lu Z, Ohara T, Song Y, Streets DG, Carmichael GR, Cheng Y (2017b) MIX: a mosaic Asian anthropogenic emission inventory under the international collaboration framework of the MICS-Asia and HTAP. *Atmos Chem Phys* 17(2):935–963
- Lin JT, Liu MY, Xin JY, Boersma KF, Spurr R, Martin R, Zhang Q (2015) Influence of aerosols and surface reflectance on satellite NO₂ retrieval: seasonal and spatial characteristics and implications for NO_x emission constraints. *Atmos Chem Phys* 15(19):11217–11241
- Madronich S (1993) The atmosphere and UV-B radiation at ground level. In *Environmental UV photobiology* (pp. 1–39). Springer, Boston
- Mahato S, Pal S, Ghosh KG (2020) Effect of lockdown amid COVID-19 pandemic on air quality of the megacity Delhi, India. *Science of the total environment* 730:139086
- Marchenko S, Krotkov NA, Lamsal LN, Celarier EA, Swartz WH, Bucselo EJ (2015) Revising the slant-column density retrieval of nitrogen dioxide observed by the Ozone Monitoring Instrument. *J Geophys Res*. <https://doi.org/10.1002/2014JD022913>
- Naja M, Bhardwaj P, Singh N, Kumar P, Kumar R, Ojha N, Sagar R, Satheesh SK, Moorthy KK, Kotamarthi VR (2016) High-frequency vertical profiling of meteorological parameters using AMF1 facility during RAWEX–GVAX at ARIES, Nainital. *Current Science* 111(1):132–140. <http://www.jstor.org/stable/24910017>
- Navinya C, Patidar G, Phuleria HC (2020) Examining effects of the COVID-19 national lockdown on ambient air quality across urban India. *Aerosol Air Qual Res* 20(8):1759–1771
- Ojha N, Naja M, Singh KP, Sarangi T, Kumar R, Lal S, Lawrence MG, Butler TM, Chandola HC (2012) Variabilities in ozone at a semi-urban site in the Indo-Gangetic Plain region: Association with the meteorology and regional processes. *J Geophys Res* 117:D20301. <https://doi.org/10.1029/2012JD017716>
- Ojha N, Naja M, Sarangi T, Kumar R, Bhardwaj P, Lal S, Venkataramani S, Sagar R, Kumar A, Chandola HC (2014) On the processes influencing the vertical distribution of ozone over the

- central Himalayas: Analysis of yearlong ozonesonde observations. *Atmos Environ* 88:201–211
- Ordóñez C, Garrido-Perez JM, García-Herrera R (2020) Early spring near-surface ozone in Europe during the COVID-19 shutdown: Meteorological effects outweigh emission changes. *Sci Total Environ* 747:141322
- Park S, Choi J (2016) Satellite-measured atmospheric aerosol content in Korea: anthropogenic signals from decadal records. *Giscience & Remote Sensing* 53(5):634–650
- Park SS, Kim J, Cho HK, Lee H, Lee Y, Miyagawa K (2012) Sudden increase in the total ozone density due to secondary ozone peaks and its effect on total ozone trends over Korea. *Atmos Environ* 47:226–235
- Peralta O, Ortíz-Alvarez A, Torres-Jardón R, Suárez-Lastra M, Castro T, Ruiz-Suárez LG (2021) Ozone over Mexico City during the COVID-19 pandemic. *Science of The Total Environment* 761:143183
- Platt U and Stutz J (2008) Differential absorption spectroscopy. In *Differential Optical Absorption Spectroscopy* (pp. 135–174). Springer, Berlin, Heidelberg
- Ravindra K, Singh T, Biswal A, Singh V, Mor S (2021) Impact of COVID-19 lockdown on ambient air quality in megacities of India and implication for air pollution control strategies. *Environ Sci Pollut Res* 28(17):21621–21632
- Rawat P, Naja M, Thapliyal PK, Srivastava S, Bhardwaj P, Kumar R, Bhattacharjee S, Venkatramani S, Tiwari SN, Lal S (2020) Assessment of vertical ozone profiles from INSAT-3D sounder over the Central Himalaya. *Curr Sci* 119(7):1113
- Rodgers CD (1976) Retrieval of atmospheric temperature and composition from remote measurements of thermal radiation. *Rev Geophys* 14(4):609–624
- Rodgers CD (1990) Characterization and error analysis of profiles retrieved from remote sounding measurements. *J Geophys Res Atmos* 95(D5):5587–5595
- Ropkins K, Tate JE (2020) Early Observations on the impact of the COVID-19 Lockdown on Air Quality Trends across the UK. *Sci Total Environ* 754:142374
- Rosenfeld D, Lahav R, Khain A, Pinsky M (2002) The role of sea spray in cleansing air pollution over ocean via cloud processes. *Science* 297(5587):1667–1670
- Sarangi T, Naja M, Ojha N, Kumar R, Lal S, Venkataramani S, Kumar A, Sagar R, Chandola HC (2014) First simultaneous measurements of ozone, CO and NO_y at a high altitude regional representative site in the central Himalayas. *J Geophys Res* 119(3):1592–1611. <https://doi.org/10.1002/2013JD020631>
- Sato TO, Sato TM, Sagawa H, Noguchi K, Saitoh N, Irie H, Kita K, Mahani ME, Zettsu K, Imasu R, Hayashida S (2018) Vertical profile of tropospheric ozone derived from synergetic retrieval using three different wavelength ranges, UV, IR, and microwave: sensitivity study for satellite observation. *Atmospheric Measurement Techniques* 11(3):1653–1668
- Schoeberl MR, Douglass AR, Hilsenrath E, Bhartia PK, Beer R, Waters JW, Gunson MR, Froidevaux L, Gille JC, Barnett JJ, Levelt PF (2006) Overview of the EOS Aura mission. *IEEE Trans Geosci Remote Sens* 44(5):1066–1074
- Silver B, He X, Arnold SR, Spracklen DV (2020) The impact of COVID-19 control measures on air quality in China. *Environ Res Lett* 15(8):084021
- Shakoor A, Chen X, Farooq TH, Shahzad U, Ashraf F, Rehman A, e Sahar N, Yan W (2020) Fluctuations in environmental pollutants and air quality during the lockdown in the USA and China: two sides of COVID-19 pandemic. *Air Qual Atmos Health* 13(11):1335–1342
- Shi X, Brasseur GP (2020) The response in air quality to the reduction of Chinese economic activities during the COVID-19 outbreak. *Geophysical Research Letters* 47(11):2020GL088070
- Sicard P, De Marco A, Agathokleous E, Feng Z, Xu X, Paoletti E, Rodriguez JJD, Calatayud V (2020) Amplified ozone pollution in cities during the COVID-19 lockdown. *Science of the Total Environment* 735:139542
- Singh RP, Kaskaoutis DG (2014) Crop residue burning: a threat to South Asian air quality. *EOS Trans Am Geophys Union* 95(37):333–334
- Singh V, Singh S, Biswal A, Kesarkar AP, Mor S, Ravindra K (2020) Diurnal and temporal changes in air pollution during COVID-19 strict lockdown over different regions of India. *Environ Pollut* 266:115368
- Srivastava P, Naja M (2021) Characteristics of carbonaceous aerosols derived from long-term high-resolution measurements at a high-altitude site in the central Himalayas: radiative forcing estimates and role of meteorology and biomass burning. *Environ Sci Pollut Res* 28(12):14654–14670
- Turquety S, Hurtmans D, Hadji-Lazaro J, Coheur PF, Clerbaux C, Josset D, Tsamalis C (2009) Tracking the emission and transport of pollution from wildfires using the IASI CO retrievals: analysis of the summer 2007 Greek fires. *Atmos Chem Phys* 9(14):4897–4913
- Veefkind JP, Aben I, McMullan K, Förster H, De Vries J, Otter G, Claas J, Eskes HJ, De Haan JF, Kleipool Q, Van Weele M (2012) TROPOMI on the ESA Sentinel-5 Precursor: A GMES mission for global observations of the atmospheric composition for climate, air quality and ozone layer applications. *Remote Sens Environ* 120:70–83
- Venkataraman C, Brauer M, Tibrewal K, Sadavarte P, Ma Q, Cohen A, Chaliyakunnel S, Frostad J, Klimont Z, Martin RV, Millet DB (2018) Source influence on emission pathways and ambient PM 2.5 pollution over India (2015–2050). *Atmospheric Chemistry and Physics* 18(11):8017–8039
- Viswanadham DV, Santosh KR (1989) Air pollution potential over south India. *Bound-Layer Meteorol* 48(3):299–313
- Wachter ED, Barret B, Flochmoën EL, Pavelin E, Matricardi M, Clerbaux C, Hadji-Lazaro J, George M, Hurtmans D, Coheur PF, Nedelec P (2012) Retrieval of MetOp-A/IASI CO profiles and validation with MOZAIC data. *Atmos Meas Tech* 5(11):2843–2857
- Wang C, Wang T, Wang P, Rakitin V (2020) Comparison and validation of TROPOMI and OMI NO₂ Observations over China. *Atmosphere* 11(6):636
- Worden J, Liu X, Bowman K, Chance K, Beer R, Eldering A, Gunson M and Worden H (2007) Improved tropospheric ozone profile retrievals using OMI and TES radiances. *GEOPHYSICAL RESEARCH LETTERS* 34:L01809. <https://doi.org/10.1029/2006GL027806>
- Xu K, Cui K, Young LH, Wang YF, Hsieh YK, Wan S, Zhang J (2020) Air quality index, indicator air pollutants and impact of COVID-19 event on the air quality near central China. *Aerosol Air Qual Res* 20(6):1204–1221
- Yarragunta Y, Srivastava S, Mitra D, Chandola HC (2021) Source apportionment of carbon monoxide over India: a quantitative analysis using MOZART-4. *Environ Sci Pollut Res* 28(7):8722–8742
- Zhao X, Griffin D, Fioletov V, McLinden C, Cede A, Tiefengraber M, Müller M, Bogner K, Strong K, Boersma F, Eskes H (2020) Assessment of the quality of TROPOMI high-spatial-resolution NO₂ data products in the Greater Toronto Area. *Atmos Meas Tech* 13(4):2131–2159
- Zhou Y, Brunner D, Boersma KF, Dirksen R, Wang P (2009) An improved tropospheric NO₂ retrieval for OMI observations in the vicinity of mountainous terrain. *Atmos Meas Tech* 2(2):401–416

Publisher's note Springer Nature remains neutral with regard to jurisdictional claims in published maps and institutional affiliations.